ADVANCED INTELLIGENT SYSTEMS
Open Access
www.advintellsyst.com

Smartphone-Embedded Artificial Intelligence-Based Regression for Colorimetric Quantification of Multiple Analytes with a Microfluidic Paper-Based Analytical Device in Synthetic Tears

Meliha Baştürk, Elif Yüzer, Mustafa Şen, and Volkan Kılıç**

Artificial intelligence (AI) and smartphones have attracted significant interest in microfluidic paper-based colorimetric sensing due to their convenience and robustness. Recently, AI-based classification of colorimetric assays has been increasingly reported. However, quantitative evaluation remains a challenge, as classification aims to categorize the color change into discrete class labels rather than a quantity. Therefore, in this study, an AI-based regression model with enhanced accuracy is developed and integrated into a microfluidic paper-based analytical device for simultaneous colorimetric measurements of glucose, cholesterol, and pH. The model is also embedded into a smartphone via a custom-designed Android application named *ChemiCheck* to complete on-site colorimetric quantification without internet access in under 1 s. The results demonstrate that the integrated system is able to sensitively detect both glucose (limit of detection [LOD]: 131 μM) and cholesterol (LOD: 217 μM), concluding the entire analysis within minutes while maintaining a maximum root mean square error of 0.386. Overall, the integrated platform holds great promise for point-of-care testing and offers numerous advantages, including easy-to-use operation, rapid response, low-cost, high selectivity, and consistent repeatability, particularly in nonlaboratory and resource-limited environments.

1. Introduction

Recently, noninvasive methods have emerged as crucial and indispensable tools in various fields, ranging from healthcare monitoring to pharmaceutical research and sports medicine.[1] Unlike invasive measurements which might pose a risk for infection and difficulty, especially for chronic patients, children/infants, and the elderly, noninvasive methods provide results without damaging tissues and thus causing no harm or discomfort.[2,3] Basically, measurements are taken in excreted fluids such as sweat, saliva, tears, and urine.[1,4,5] However, they inherently lack the same level of accuracy and reliability as invasive measurements.[6,7] Despite the positive contributions of technological advancements to the sensitivity and accuracy in noninvasive methods, there remains a necessity for further innovation and research. Various detection principles have been successfully used for the noninvasive measurement of different biologically relevant molecules;[3,8,9] among them, colorimetric and electrochemical detection methods have attracted the most attention due to their accessibility, sensitivity, versatility, and suitability for healthcare applications. Compared to electrochemical methods, colorimetric detection offers simplicity and ease of interpretation because the presence of the target species can be visibly determined.[10] It also allows high-throughput analysis and can be adapted in resource-limited settings. Colorimetric detection can be easily integrated into microfluidic paper-based analytical devices (μPAD) which offer new directions for simple, low-cost, and portable diagnostic/analytical applications.[11,12] Despite the advantages outlined, colorimetric detection has its own challenges. Notably, the color change interpretation is greatly affected by camera optics and ambient light, reducing the sensitivity of the measurement. Recently, artificial intelligence (AI) has been successfully applied to address this issue and interpret color changes robustly to achieve reliable analysis, even in complex and variable sample matrices.[13–16]

AI-driven techniques have been employed in numerous tasks, including classification[17,18] and regression analyses.[19]

M. Baştürk, V. Kılıç
Department of Electrical and Electronics Engineering Graduate Program
Izmir Katip Celebi University
Izmir 35620, Turkey
E-mail: volkan.kilic@ikcu.edu.tr

E. Yüzer, M. Şen
Department of Biomedical Engineering Graduate Program
Izmir Katip Celebi University
Izmir 35620, Turkey
E-mail: mustafa.sen@ikcu.edu.tr

The ORCID identification number(s) for the author(s) of this article can be found under https://doi.org/10.1002/aisy.202400202.

DOI: 10.1002/aisy.202400202

Classification categorizes data into predefined groups or classes[20] while regression is employed to forecast the relationship between a dependent variable and one or more independent variables.[21] Machine learning (ML) and deep learning (DL), subsets of AI, are techniques for classification problems that have found widespread applications in colorimetric analysis due to their advantages such as autonomous learning from data and automatic decision-making.[11] Although ML techniques require less processing power and small dataset, DL techniques offer advantages to handle more complex classification problems with their neural network-based architecture.[22–24] An issue with classification-based techniques in colorimetric analysis is that they assign predefined classes rather than providing a certain quantity in a measurement.[25] To address this issue, regression-based techniques have been proposed to compute intermediate concentration values.[12] Conventional regression approaches rely on a calibration curve that relates intensity to concentration. The calibration curve, while accurate under controlled conditions, lacks robustness to changes in camera optics and illumination, requiring recalibration for new conditions.[26,27] In this regard, due to their ability to learn how to fit inputs based on features extracted from color information, these limitations have been readily addressed with AI-based regression approaches such as multiple linear, support vector, decision tree, random forest, and deep neural network (DNN).[28] Among these approaches, DNN has demonstrated promising performance, due to its ability to handle complex relationships of input features with the neural network structure.[29] In addition, advancements in AI coding libraries together with the increasing capability in computer processing have enabled the integration of AI models into custom-designed cloud-based smartphone applications such as GlucoSensing,[13] Hi-perox Sens,[15] and ChemTrainer.[30] However, cloud-based systems require continuous server operation, leading to high operational costs. Furthermore, varying internet speeds may result in data transfer delays, potentially affecting analysis outcomes.

Glucose serves as the key indicator for diabetes, with high blood glucose levels being the defining characteristic of both Type 1 and Type 2 diabetes. People with diabetes often experience dyslipidemia and altered tear pH, which increase the risk of cardiovascular diseases and complications like diabetic ketoacidosis and dry eye syndrome.[31–33] Monitoring glucose, cholesterol, and pH in tears provides a comprehensive and noninvasive method for managing diabetes and its associated risks. Tears, easily accessible bodily fluids with fewer interferents than saliva, sweat, and urine,[34] offer valuable health insights and can be used for noninvasive monitoring of the three analytes. Here, an AI-based regression model was developed and embedded into a smartphone application to quantify glucose, cholesterol, and pH levels simultaneously in synthetic tears using a μPAD. Initially, μPADs with three detection zones were fabricated using wax printing. Subsequently, a dataset was created for training AI-based regression models using images of μPADs captured under seven lighting conditions with smartphones from different brands, enhancing robustness to variations in illumination and camera optics. Based on performance comparisons of AI-based regression models, the DNN-based regression was embedded in a user-friendly application called *ChemiCheck*. The performance of the integrated system was evaluated in tears with varying levels of glucose, cholesterol, and pH (**Figure 1**). The results demonstrated that the integrated system offered significant advantages for colorimetric quantification of multiple analytes, with potential applications in nonlaboratory and resource-limited settings.

2. Experimental Section

2.1. Materials

Albumine from human serum (HSA, $\geq$ 96%) (Amresco, USA), Whatman qualitative filter paper grade 1 (GE Healthcare, UK),

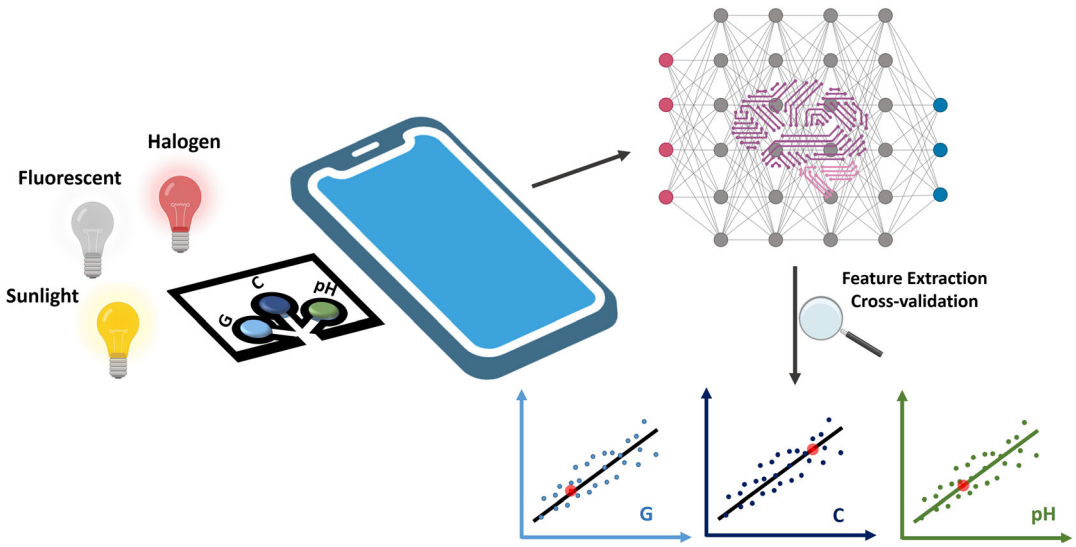

Figure 1. A schematic illustration of the AI-based regression enhanced quantitative detection of glucose, cholesterol, and pH in synthetic tears. Color change in the detection zones of the PAD was imaged under various combinations of fluorescent, halogen, and sunlight sources using smartphone cameras of different brands.

and universal pH indicator solution (Izmir Teknik Kimya, Turkey) were used. The following chemicals were purchased from Sigma Aldrich, USA; glucose oxidase (GOx) from Aspergillus niger ($\geq$ 1920 units/mg), cholesterol oxidase (ChOx) ($\geq$ 50 units/mg), peroxidase from horseradish (HRP) ($\geq$ 250 units/mg), 3,3,5,5-tetramethylbenzidine (TMB), D(+)-glucose ($\geq$ 99%), cholesterol ($\geq$ 99%), NaOH ($\geq$ 98%), HCl (37%), NaCl ($\geq$ 99%), $CaCl_2$ ($\geq$ 97%), KCl ($\geq$ 99%), NH_4Cl ($\geq$ 99%), lactic acid (LA) ($\geq$ 85%), sucrose ($\geq$ 99.5%), uric acid (UA) ($\geq$ 99%), ascorbic acid (AA) ($\geq$ 99%), and dopamine (DA) ($\geq$ 97%).

2.2. Design and Fabrication of μPADs

The microfluidic device, specifically the μPAD used for detecting glucose, cholesterol, and pH, was fabricated using a wax printing technique, as outlined by Carrilho and Lu (2009). Initially, the device design was created using Microsoft PowerPoint 2021 (version 16) software, ensuring precise layout and dimensions of the detection zones and fluidic channels. The design had three circular separate detection zones with a diameter of 2 mm for each molecule. The μPAD had a channel width and length of $\approx$4 and 8 mm for delivery of sample to the detection zones, respectively. This design was then transferred onto Whatman filter paper (grade 1) using a wax printer (Xerox ColorQube 8900, Xerox Corporation, USA). The fabrication process involved placing the printed filter paper on a hot plate set to 180 °C for 180 s. During this step, the wax on the paper melted and impregnated the porous structure of the filter paper. This infiltration of molten wax into the paper pores served two critical functions: first, it defined the detection zones where biochemical reactions would occur and second, it created hydrophobic channels that directed and controlled the flow of fluids through the device. Next, to enable the colorimetric detection of glucose and cholesterol on μPADs, specific modifications were implemented within the detection zones. Initially, 0.8 μL of TMB and 1 μL of an enzyme mixture were applied. This enzyme mixture consisted of 50 U mL^{-1} HRP (horseradish peroxidase) paired with either 180 U mL^{-1} GOx for glucose detection or 200 U mL^{-1} ChOx for cholesterol detection. After each addition of the enzyme mixture or TMB solution, the μPADs were allowed to air dry at room temperature. This step ensures the proper immobilization and activation of the enzymes within the detection zones, crucial for subsequent colorimetric reactions. For pH detection, the μPADs were similarly prepared by applying 0.8 μL of a universal pH indicator solution to the designated detection zone. The indicator solution was left to dry under ambient conditions. This modification equipped the μPADs to visually indicate the pH of a sample through distinctive color changes, contributing to the device's versatility in analytical applications.

2.3. Image Acquisition

Varying levels of glucose (0, 0.1, 0.25, 0.5, 1, 2.5, 5, and 10 mM), cholesterol (0, 0.1, 0.25, 0.5, 1, and 5 mM), and pH (4, 5, 6, 7, 8, and 9) were tested for colorimetric detection. All chemicals were dissolved and tested in synthetic tears which were prepared as described in ref. [35]. The performance and reliability of AI-based models are directly linked to the number of images in a dataset, as increased data enhances the training accuracy of models. In this regard, images were captured under various scenarios, involving three distinct lighting sources: halogen (H), fluorescent (F), and sunlight (S) with color temperatures of 2700 K (warm), 4000 K (neutral), and 6500 K (cold), respectively. To ensure a comprehensive dataset, seven illumination conditions (H, F, S, HF, HS, FS, and HFS) were created by combining these lighting sources in various configurations. Moreover, to replicate orientation scenarios, images were taken from five distinct angles (30°, 60°, 90°, 120°, and 150°) relative to the vertical axis between the μPAD and the smartphone camera. The light sources were positioned at a distance of 40 cm from the smartphones, with 9 cm spacing between each lamp source. Images were taken at an incidence angle of 35° between the light sources and the μPAD. Additionally, four different smartphone camera optics were utilized during image capture to ensure comprehensive coverage. The camera specifications are given in **Table 1** for two iOS (iPhone 7 Plus and iPhone SE) and two Android smartphones (Oppo A5 2020 and LG G6 (H870)).

Table 1. Camera properties of the smartphones used for capturing images.

Smartphone brand	Image resolution	Optics	Camera resolution
iPhone 7 Plus	4032 × 3024	$f/1.8$	12 MP
iPhone SE	1136 × 640	$f/2.2$	12 MP
Oppo A 5 2020	4000 × 3000	$f/1.8$	12 MP
LG G 6 (H 870)	2880 × 1440	$f/2.4$	13 MP

As each regression model needs to be trained effectively for the target analytes, individual datasets were prepared for glucose, cholesterol, and pH. For the dataset of glucose, 280 images were first captured via a smartphone using eight concentration levels, seven lighting conditions, and five different angles. The capturing was then repeated across four smartphones and three different time intervals (30 s, 5, and 10 min), resulting in 3360 images. All three detection zones of the μPAD were utilized for glucose detection, enabling the collection of a larger number of images. This approach resulted in the acquisition of 10080 patches in total. The whole dataset was divided into three subdatasets based on time intervals (30 s, 5, and 10 min) to have a time-dependent analysis, ensuring low error in calculation. The same process was repeated for both cholesterol and pH measurements to obtain separate datasets for each analyte. These subdatasets were divided into training and test sets using an 80:20 ratio. Additionally, 20% of the training set was further separated to create a validation set as these ratios were commonly employed in AI applications.[36] The dataset was transferred to a computer for preprocessing in MATLAB (R2023a, MathWorks Inc.). The region of interest (ROI) zones, where color changes become apparent due to the enzymatic reactions, were cropped to extract features for the training of AI-based regression models.

2.4. AI-Based Regression

Regression is used to determine the value of a dependent variable based on changes in independent variables by modeling complex

relationships through linear and nonlinear approaches.[37] Unlike ML classifiers, regression offers precise decimal predictions. The characteristics of the data and modeling requirements play a crucial role in the selection of approaches, including linear, nonlinear, and multiple regressions.[36] In this study, DNN-based regression was utilized due to its capacity to handle both linear and nonlinear data through its multilayer neural network structure, enabling the learning of more complex and high-level features.

There are several challenges for AI-based regression models including model generalization issues, imbalance of data sets, and the impact of interferers. Addressing these challenges is crucial to ensure that the proposed system is robust and highly accurate in regression analysis. To achieve this, blurry or unfocused images were retaken to account for interferences caused by ambient light conditions and human error. This capturing process was repeated with four different smartphones, each with different camera optics and image processing, running two different operating systems (iOS and Android). This allowed us to consider systemic and operational interferences, such as hardware limitations and software implementation. Additionally, we captured the same number of images for each concentration to avoid dataset imbalance and used image augmentation to further increase diversity. During the training, regularization techniques and early stopping were implemented to prevent overfitting. Model hyperparameters such as epoch number, batch size, activation functions, optimizers, loss functions, and the number of layers were optimized using grid search techniques.

The AI-based regression model consists of two steps: 1) feature extraction from the image; and 2) colorimetric regression with DNN (**Figure 2**). First, 12 color channels including red-green-blue (RGB), hue-saturation-value (HSV), lightness, green-red, blue-yellow (L*a*b*), and luminance-chrominance1-chrominance2 (YUV) of images were obtained. Then, average, standard deviation, and kurtosis of each channel were calculated and stored in an Excel spreadsheet (.xlsx) file to train 12 different regression models (**Table 2**). DNN regression was embedded into the *ChemiCheck* application due to its superior performance. It consisted of input and six hidden and output layers where the dimensions gradually reduced from 1024 to 1. A rectified linear unit (ReLU) was used as a nonlinear activation function at the end of each layer.

Table 2. Comparison of glucose regression models for 10 min.

Regression models	MSE	MAE	R^2	RMSE
Linear regression	0.458	0.497	0.957	0.676
Elastic net regression	0.875	0.702	0.917	0.935
Ridge regression	0.473	0.495	0.955	0.688
Lasso regression	0.930	0.732	0.912	0.964
Decision tree regression	0.255	0.119	0.976	0.505
Random forest regression	0.143	0.164	0.987	0.379
Support vector regression	0.810	0.556	0.923	0.900
Gradient boosting regression	0.200	0.257	0.981	0.448
K-Nearest neighbors regression	0.193	0.187	0.982	0.439
AdaBoost regression	0.622	0.671	0.941	0.789
XGBoost regression	0.160	0.178	0.985	0.400
DNN regression	0.045	0.115	0.996	0.213

2.5. Smartphone Application: ChemiCheck

ChemiCheck, a smartphone application, was developed to perform colorimetric analysis of synthetic tears, enabling the quantification of glucose, cholesterol, and pH with decimal

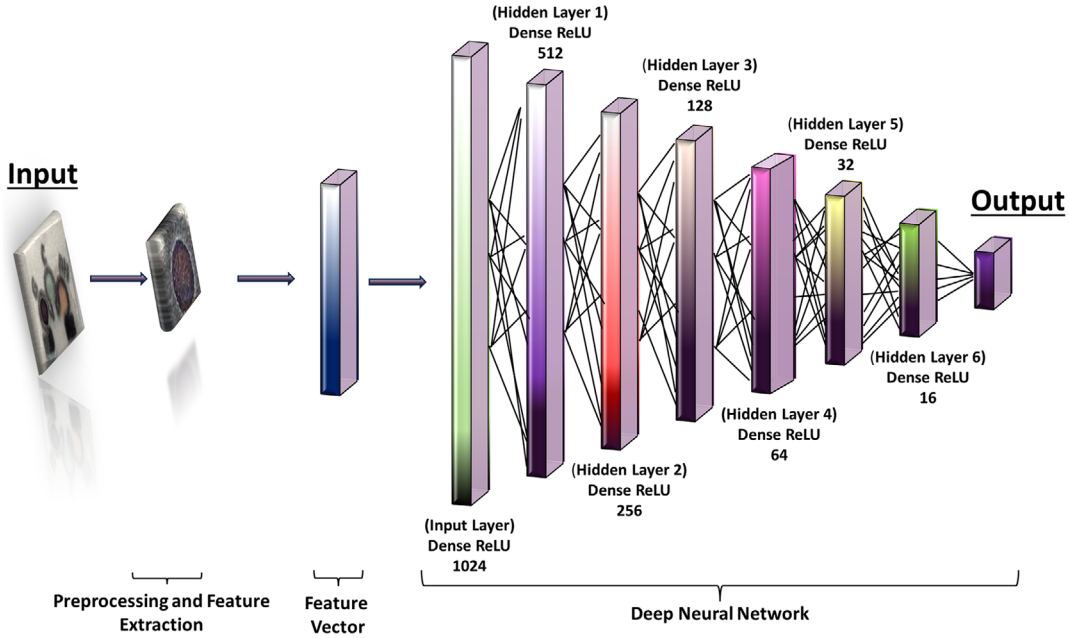

Figure 2. General structure of the proposed DNN.

precision. Embedding the proposed DNN-based regression resulted in reducing the analysis time to less than 1 s. To integrate the trained DNN-based regression model into Android smartphones, the TensorFlow-Lite (.tflite) library was used to ensure compatibility with mobile devices. The model, initially stored in a Hierarchical Data Format (HDF,.h5 file), was subsequently transformed into a.tflite file format to enable its integration into the smartphone application. Then three different.tflite files for glucose, cholesterol, and pH were embedded in the ChemiCheck application. Users can select or capture an image, adjust the ROI, and access quantification results for glucose, cholesterol, and pH with their respective processing times.

2.6. Selectivity

The selectivity of the μPADs toward glucose and cholesterol was tested using the following chemical species, glucose, cholesterol, NH_4Cl, DA, sucrose, LA, UA, AA, and blank (control) synthetic tears. All species were prepared in synthetic tears at a concentration of 1 mM. The RGB intensity of color change data for each test at 5 min was used for comparison.

3. Results and Discussion

Here, a smartphone application incorporating an AI-based regression model was integrated with a μPAD for offline colorimetric measurement of glucose, cholesterol, and pH in synthetic tears. A special design, incorporating a sample collection pad and three detection zones, was printed onto Whatman filter paper (grade 1) through wax printing to fabricate μPADs for sample retrieval without the need for an external tool (**Figure 3**). Hydrophobic channels created by the wax printing method define boundaries and limit the path of the liquid so that the sample can be transported to the detection zones via capillary force. The width of the sample collection pad was optimized to ensure easy and fast passage of liquid through the channels before use. The present μPAD has a sample collection width of 0.5 cm and can draw less than 20 μL of sample in under 30 s. Glucose and cholesterol were both detected colorimetrically using the chromogenic agent TMB. Thus, the uppercase letters 'G' and 'C' were employed to differentiate between the detection zones for these two molecules (Figure 3a). The detection of glucose was achieved through a sequential reaction process in which GOx first catalyzes the oxidation of D-glucose into gluconolactone.[13] A similar sequential reaction was employed for the detection of cholesterol in which case another oxidase called ChOx was used to catalyze the conversion of cholesterol to cholest-4-en-3-one. Both enzymatic reaction produces H_2O_2 as a byproduct which is then used by HRP to oxidize the chromogenic agent TMB, forming a blueish color change in both detection zones. In the third detection zone, pH determination was performed using the universal pH indicator, which changes color from red to indigo as the pH of the sample increases. As shown in Figure 3b,c, glucose and cholesterol as well as the pH of the synthetic tears can be separately and simultaneously detected using a single μPAD. Next, the μPADs were tested with varying concentrations/levels of glucose, cholesterol, and pH. Visible color changes were observed for all three molecules in tears at 30 s, 5, and 10 min, as depicted in **Figure 4** and S1, Supporting Information. For the AI-based regression models, it is necessary to have a comprehensive dataset created for challenging scenarios. This includes capturing images under diverse lighting conditions with various orientations and utilizing different camera optics to ensure repeatability across different smartphones. Therefore, the images of the μPADs were taken under seven different lighting conditions at different angles using four smartphones of different brands (iPhone 7 Plus, iPhone SE, Oppo A5 2020, LG G6 (H870)) (Table 1).

Following the preparation of datasets as detailed in Section 2.3, the regression models listed in Table 2, S1 and S2, Supporting Information, were tested for glucose, cholesterol, and pH to establish a performance benchmark for comparison. Among the models, DNN-based regression demonstrated superior performance across multiple metrics such as mean squared error (MSE), mean absolute error (MAE), R^2, and root mean square error (RMSE). MSE measures the average squared difference between the actual and predicted values of a regression model. For each observation, the squared difference between the actual and predicted values is calculated, and the sum of these squared differences is divided by the number of observations. MAE measures the average absolute difference between the actual and predicted values of a regression model. R^2 calculates the proportion of the variance in the dependent variable that is predictable from the independent variables. RMSE is the square

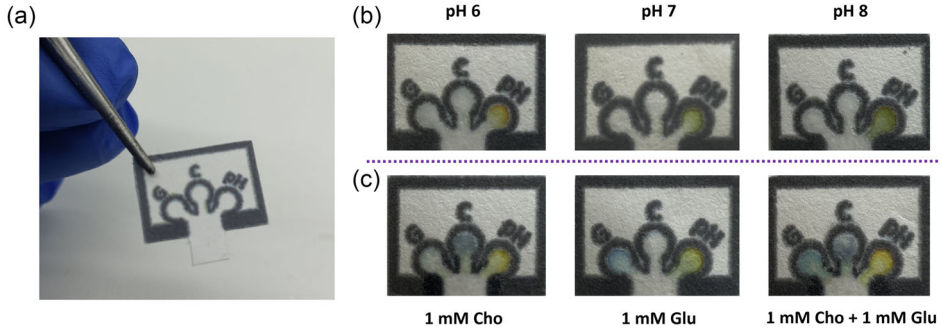

Figure 3. a) Image of a ready-to-use μPAD along with the b,c) results showing that the µPAD can be used for the simultaneous detection of glucose, cholesterol, and pH. The experiments in (b) were carried out in synthetic tear solutions with different pH levels, while those in (c) were conducted in synthetic tears supplemented with 1 mM of glucose and cholesterol.

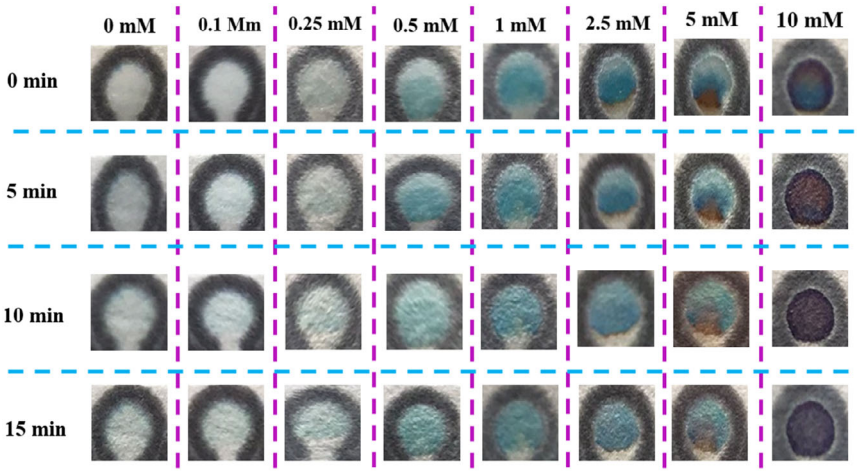

Figure 4. Images of μPADs showing visually observable color changes with varying concentrations of glucose in tears at 30 s, 5, and 10 min.

root of the average squared differences between the actual and the predicted values. The DNN-based regression model was trained using the parameters of "adam" optimizer and MSE loss function for 500 epochs with a batch size of 32 utilizing the Tensorflow Keras library in Python programming language. These parameters were found to be adequate based on extensive experiments. The performance comparison of the DNN-based regression model at all minutes for glucose, cholesterol, and pH is shown in **Table 3**. The most promising results were observed in cholesterol, achieving an MSE of 0.008 within 30 . While the optimal result for glucose was achieved at 10 min, all performance metrics remained largely consistent throughout the 10-min duration. Thus, it is concluded that the integrated system can be reliably and safely applied for the quantification of glucose across all three time points. Unlike glucose and cholesterol, the color change for pH sensing was less pronounced. For instance, the transitions between pH 4–5 and pH 8–9 were not as clearly discernible as those between pH 5 and 8 (Figure S1, Supporting Information). Consequently, the performance metrics for pH were slightly inferior to those for glucose and cholesterol. Nevertheless, the integrated system proves reliable for pH sensing in tears (ranging from pH 5 to 8), as the DNN-based regression successfully identified the color change, and the alteration between pH 5 and 8 was visually noticeable. Moreover, the proposed DNN-based regression was also compared with state-of-the-art approaches tested on various samples including blood plasma, blood serum, phosphate buffered saline (PBS), soil, Britton–Robinson (BR) buffer, H_2O, and red cabbage in **Table 4**. Comparative analysis has revealed that the proposed model outperforms the state-of-the-art approaches. The accuracy of the proposed DNN-based regression approach was also compared to the traditional calibration curve method. Images taken by four different smartphone brands under the same lighting conditions (F) and at the same angle (90°) were used to obtain calibration curves based on RGB intensity for 10 mM glucose, 0.5 mM cholesterol, and pH 6. As shown in Table S3, Supporting Information, the DNN-based regression approach provided results closest to the ground truth (GT) values. Significant fluctuations were observed among the smartphones,

Table 3. Performance of DNN regression model for glucose, cholesterol, and pH at all mins.

	Times [min]	MSE	MAE	R^2	RMSE
Glucose	0.5	0.049	0.119	0.996	0.220
	5	0.802	0.175	0.925	0.895
	10	0.045	0.115	0.996	0.213
Cholesterol	0.5	0.008	0.060	0.997	0.089
	5	0.013	0.062	0.995	0.114
	10	0.018	0.087	0.993	0.135
pH	0.5	0.149	0.302	0.948	0.386
	5	0.102	0.203	0.964	0.319
	10	0.202	0.337	0.931	0.450

Table 4. State-of-the-art comparison for glucose, cholesterol, and pH.

		Sample	MSE	MAE	R^2	RMSE
Glucose	[12]	Blood plasma	2.096	–	0.970	–
	[36]	Blood serum	0.352	0.438	–	0.594
	[45]	Pbs	0.170	0.200	0.950	0.410
	Ours	Synthetic tears	0.045	0.115	0.996	0.213
Cholesterol	[46]	Blood serum	–	–	0.930	15.900
	[47]	PBS	–	–	0.987	–
	[48]	Commercial kit sample	–	–	0.995	1.530
	[49]	Blood	–	–	0.999	0.337
	Ours	Synthetic tears	0.008	0.060	0.997	0.089
pH	[50]	Soil	–	–	0.825	0.541
	[51]	BR buffer	0.130	0.242	0.991	0.361
	[52]	H_2O	–	–	0.952	0.219
	[53]	Red cabbage	–	–	0.998	0.115
	Ours	Synthetic tears	0.102	0.203	0.964	0.319

particularly for cholesterol and pH, demonstrating the high accuracy of the proposed system. Furthermore, the limit of detection (LOD) values of the integrated system for glucose and cholesterol were determined using the RGB data from images captured by an iPhone 7 Plus under HFS illumination Belgrade, Serbia, 29 Aug - 2 Sep (LOD = $3*\sigma$/Slope). The system achieved LOD values of 131 μM for glucose and 217 μM for cholesterol. Importantly, the integrated system operates based on features rather than a traditional calibration curve. Therefore, it should be noted that the LOD values derived from the features used to train the AI algorithms cannot be directly calculated. Nevertheless, LOD values obtained from respective calibration curves still demonstrate the system's ability to detect low concentrations of glucose and cholesterol.

The smartphone application *ChemiCheck* was demonstrated step by step with screenshots in **Figure 5**. The homepage has 'gallery' and 'camera' buttons for image selection and capturing, respectively. An image can be selected from the gallery, as in Figure 5b, or a new image can be captured using the camera. Figure 5c shows the cropping screen where the user can make the necessary scaling and orientation changes for ROI (Figure 5d). Depending on the ROI zone, the 'GLU' (Figure 5e), 'CHO' (Figure 5f), and 'pH' (Figure 5g) buttons can be tapped to access glucose, cholesterol, and pH measurements as shown in Figure 5h. The process involves colorimetric analysis of glucose, cholesterol, and pH using images from the gallery. *ChemiCheck* accurately quantified the levels of glucose, cholesterol, and pH in synthetic tears using the proposed

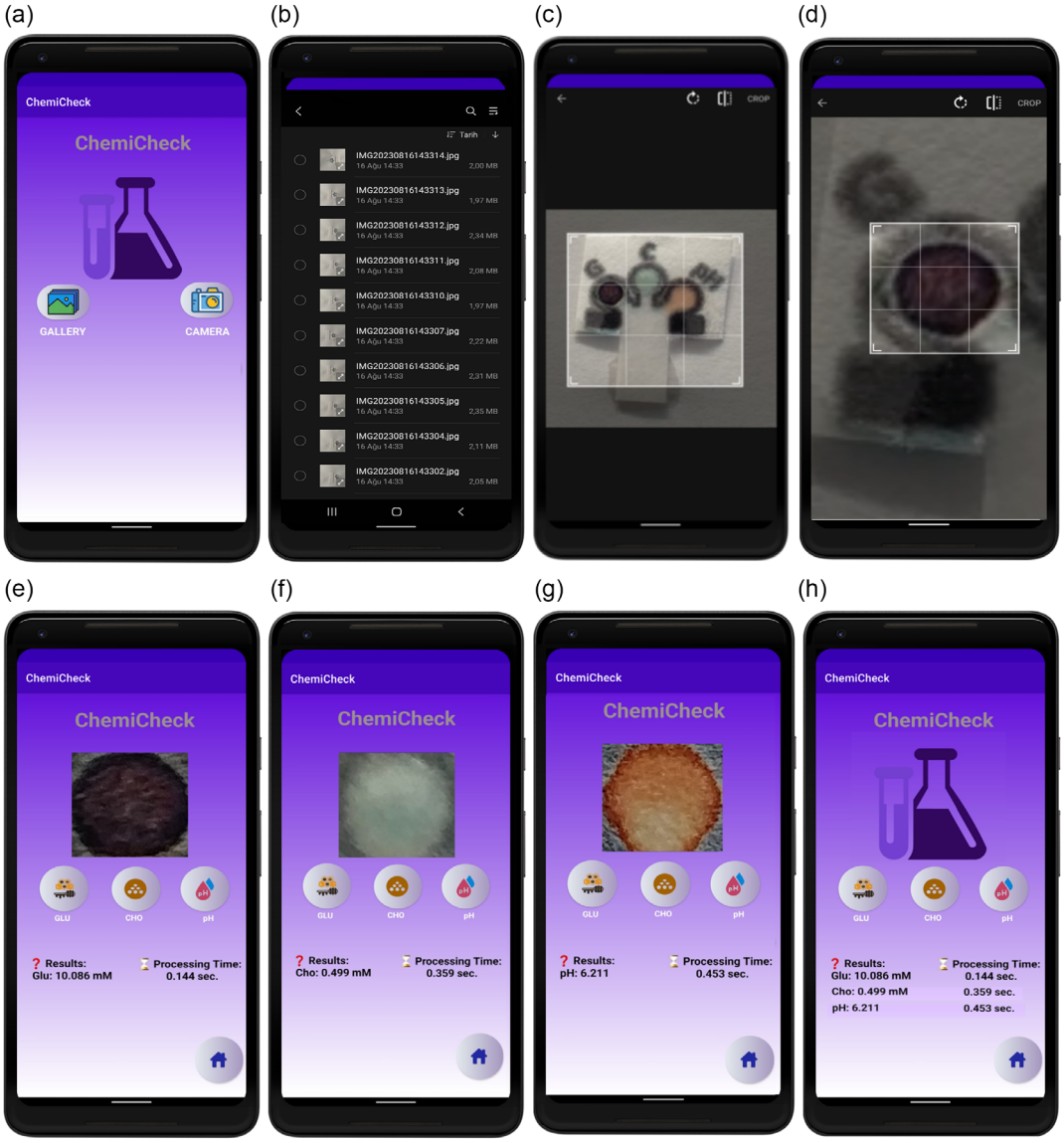

Figure 5. The steps for colorimetric glucose analysis in *ChemiCheck*. a) The homepage of *ChemiCheck*. The user can select an image from the b) gallery or capture a new image using the smartphone camera. After selecting the image from the gallery, the user can use c) cropbox. d) The scaling and orientation. e,f,g) The user can choose glucose, cholesterol, and pH for colorimetric analysis. The *ChemiCheck* was tested with synthetic tears containing 10 mM glucose (e) and 0.5 mM cholesterol (f) at pH 6 (g). The results and processing times are shown in h).

DNN-based regression model under 1 s. Even though the results for all three measurements were shown with three decimal places, it is advisable to omit the last two digits due to sensitivity considerations. The application has a simple and user-friendly interface and offers offline analysis for inexperienced users in remote areas. Several studies have demonstrated the feasibility of colorimetrically detecting various biomarkers such as ascorbic acid, Ca^{2+}, protein, and nitrite in tears.[38,39] Therefore, the device can potentially be adapted for detecting these molecules by incorporating relevant detection reagents into the existing detection zones. While it is feasible to detect additional analytes by adding more detection zones to the device, further miniaturization of these zones may impede sample delivery and complicate the detection process. Alternatively, enlarging the device to accommodate more detection zones with current dimensions is possible; however, it would also extend the sample delivery channel; thereby, regression and classification are two fundamental types of supervised learning tasks in AI. Regression provides quantitative and continuous variables for analysis, while classification assigns discrete categories. Classification models can often be more robust to outliers compared to regression models. However, converting continuous data into discrete categories can result in information loss. Additionally, classification models can struggle with imbalanced datasets, where one class is much more frequent than others, potentially causing biased predictions. Therefore, regression was employed in this study to leverage its strengths in obtaining quantitative and continuous variables for colorimetric analysis.

Next, the selectivity of the platform was tested against several interfering species including NH_4Cl, DA, sucrose, LA, UA, and AA at 1 mM. The color intensity in both glucose (**Figure 6**a) and cholesterol (Figure 6b) detection zones did not significantly change from that of blank synthetic tears. However, the presence of glucose and cholesterol at 1 mM resulted in a drastic change in color intensity, proving the selective detection ability of the platform for the two molecules. The device achieves high selectivity primarily due to the enzymes' specificity toward their respective analytes (glucose, cholesterol, pH). For example, glucose oxidase catalyzes the oxidation of glucose, generating hydrogen peroxide as a detectable byproduct through colorimetric methods. Similarly, cholesterol oxidase and pH-sensitive indicators demonstrate specificity in their reactions with target analytes. Furthermore, the design ensures that the borders of the detection zones prevent interference between the detection of different analytes, thereby enhancing the device's selectivity. It is important to note that since only TMB and various enzymes are used for colorimetric detection, the long-term stability of these μPADs largely depends on enzyme stability. Enzymes can remain stable for months depending on storage conditions, and their stability can be further enhanced with the use of certain additives.[40,41]

(c)

	Glucose (mM)	Cholesterol (mM)	pH
V.1	0.343	0.117	6.62
V.2	0.271	0.128	6.7
V.3	0.339	0.249	6.67

Figure 7. Real sample testing results. The screenshot of the a) analysis results and the b) μPAD image of the first volunteer (V.1) along with the c) results of all volunteers (V.1, V.2, and V.3).

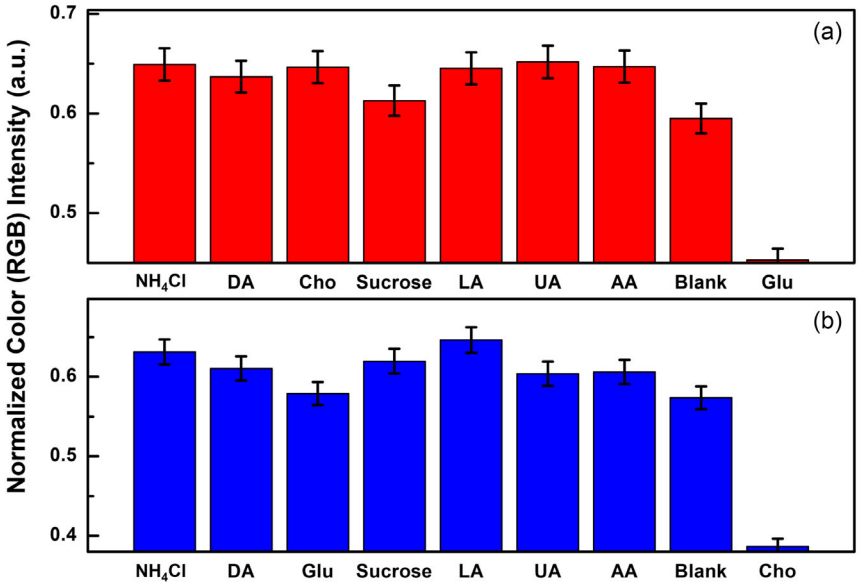

Figure 6. Selectivity test results of a) colorimetric glucose and b) cholesterol sensors.

Lastly, the integrated system was tested on three volunteers aged below 26 years. All volunteers were provided with a consent form and informed about the study. Before application, the skin beneath their eyes was cleansed. A tear stick was used to stimulate tear production, and the resulting tears were carefully collected using the sample collection pad of μPADs. The color change at 5 min was analyzed by the system (**Figure 7**a,b). Average values for glucose, cholesterol, and pH were determined as shown in Figure 7c: 0.343 ± 0.32 for glucose, 0.165 ± 0.06 for cholesterol, and 6.66 ± 0.03 for pH. The glucose and pH values closely matched those reported by other groups.[42,43] The cholesterol level was slightly lower than that reported in ref. [44], which is normal because cholesterol levels in tears may vary depending on age, diet, hydration, and overall health.

4. Conclusion

In this study, a new implementation of a smartphone-embedded DNN-based regression model relying on a color change in μPADs was proposed to quantify glucose, cholesterol, and pH levels in synthetic tears. First, different AI-based regression models were trained with the images of μPADs captured in seven lighting conditions using four smartphones of different brands for improved robustness against lighting variation and camera optics. Next, the DNN-based regression model which demonstrated superior performance was embedded into a smartphone application called *ChemiCheck*, enabling the quantification of each analyte in less than one second. The integrated system can simultaneously and sensitively quantify the three analytes at physiologically relevant concentration levels in synthetic tears within minutes, achieving a maximum RMSE of 0.386. To the best of our knowledge, this is the first study that uses an AI-based regression model for the quantification of multiple analytes using a paper-based sensor. The proposed system can easily be applied to noninvasive clinical monitoring in remote and resource-limited settings, owing to its various advantages such as straightforward operability, cost-effectiveness, and robust performance.

Supporting Information

Supporting Information is available from the Wiley Online Library or from the author.

Acknowledgements

This research was partly supported by the Scientific and Technical Research Council of Turkey (project no. 123M411).

Conflict of Interest

The authors declare no conflict of interest.

Author Contributions

Meliha Bastürk: Validation (equal); Visualization (equal); Writing—original draft (equal). **Elif Yüzer**: Visualization (equal); Writing—original draft (equal). **Mustafa Şen**: Funding acquisition (lead); Writing—original draft (equal); Writing—review & editing (equal). **Volkan Kılıç**: Conceptualization (equal); Methodology (equal); Supervision (equal); Validation (equal); Writing—review & editing (equal).

Data Availability Statement

The data that support the findings of this study are available from the corresponding author upon reasonable request.

Keywords

cholesterol, deep neural network-based regression models, glucose, microfluidic paper-based analytical devices, pH, smartphone applications, tears

Received: March 14, 2024
Revised: July 31, 2024
Published online: August 18, 2024

[1] M. Falk, C. Psotta, S. Cirovic, S. Shleev, *Sensors* **2020**, *20*, 6352.
[2] F. Ferrara, S. Zoupanou, E. Primiceri, Z. Ali, M. S. Chiriacò, *Biosens. Bioelectron.* **2022**, *196*, 113698.
[3] L. Tang, S. J. Chang, C.-J. Chen, J.-T. Liu, *Sensors* **2020**, *20*, 6925.
[4] A. Alves, A. Kucharska, C. Erratico, F. Xu, E. Den Hond, G. Koppen, G. Vanermen, A. Covaci, S. Voorspoels, *Anal. Bioanal. Chem.* **2014**, *406*, 4063.
[5] M. Esteban, A. Castaño, *Environ. Int.* **2009**, *35*, 438.
[6] K. Patel, G. Sebastiani, *JHEP Rep.* **2020**, *2*, 100067.
[7] N. Lindner, A. Kuwabara, T. Holt, *Syst. Rev.* **2021**, *10*, 145.
[8] Y. Zou, Z. Chu, J. Guo, S. Liu, X. Ma, J. Guo, *Biosens. Bioelectron.* **2023**, *225*, 115103.
[9] M. Sen, M. Oguz, I. Avc, *Talanta* **2024**, *268*, 125341.
[10] Y. Wu, J. Feng, G. Hu, E. Zhang, H.-H. Yu, *Sensors* **2023**, *23*, 2749.
[11] E. Yüzer, V. Dogan, V. Klç, M. Sen, *Sens. Actuators, B* **2022**, *371*, 132489.
[12] S. Ghateii, A. Jahanshahi, *Sens. Actuators, B* **2024**, *400*, 134835.
[13] Ö. B. Mercan, V. Klç, M. Sen, *Sens. Actuators, B* **2021**, *329*, 129037.
[14] M. Sen, E. Yüzer, V. Dogan, I. Avc, K. Ensarioglu, A. Aykaç, N. Kaya, M. Can, V. Klç, *Microchim. Acta* **2022**, *189*, 373.
[15] V. Dogan, E. Yüzer, V. Klç, M. Sen, *Analyst* **2021**, *146*, 7336.
[16] G. D. Ozdemir, M. A. Ozdemir, M. Sen, U. K. Ercan, *Adv. Intell. Syst.* **2024**, 2400029.
[17] Ö. Çayl, V. Klç, A. Onan, W. Wang, in *2022 30th European Signal Processing Conf. (EUSIPCO)*, IEEE, Belgrade, Serbia **2022**, pp. 1–4.
[18] M. Agral, V. Kilic, A. Onan, E. M. Koç, A. M. Koç, R. E. Büyüktoka, T. Acar, Z. Adbelli, *Int. J. Imaging Syst. Technol.* **2023**, *33*, 776.
[19] M. Redmile-Gordon, E. Armenise, R. P. White, P. Hirsch, K. Goulding, *Soil Biol. Biochem.* **2013**, *67*, 166.
[20] S. Fuentes, E. Hernández-Montes, J. Escalona, J. Bota, C. G. Viejo, C. Poblete-Echeverra, E. Tongson, H. Medrano, *Comput. Electron. Agric.* **2018**, *151*, 311.
[21] S.-J. Kim, J. Y. Lee, S.-R. Yoon, H.-W. Lee, J.-H. Ha, *J. Food Eng.* **2019**, *240*, 65.
[22] S. Uçkun, M. Agral, V. Klç, *Avrupa Bilim Teknol. Derg.* **2023**, *50*, 105.
[23] M. Agral, M. U. Soydemir, A. Gökçen, S. Sahin, *Avrupa Bilim Teknol. Derg.* **2021**, *26*, 358.
[24] B. Makav, V. Klç, in *11th Int. Conf. on Electrical and Electronics Engineering (ELECO)*, IEEE, Bursa, Turkey **2019**, pp. 1–5.

[25] Z. Xu, K. Wang, M. Zhang, T. Wang, X. Du, Z. Gao, S. Hu, X. Ren, H. Feng, *Sens. Actuators, B* **2022**, *359*, 131590.
[26] G. A. Helfer, V. S. Magnus, F. C. Böck, A. Teichmann, M. F. Ferrão, A. B. D. Costa, *J. Braz. Chem. Soc.* **2017**, *28*, 328.
[27] A. Vaquer, E. Barón, R. de la Rica, *Analyst* **2021**, *146*, 3273.
[28] T. Lee, H.-T. Lee, J. Hong, S. Roh, K. Lee, Y. Choi, Y. Hong, H.-J. Hwang, G. Lee, *Anal. Methods* **2022**, *14*, 4749.
[29] Y. Chen, K. Yao, B. Zhu, Z. Gao, J. Xu, Y. Li, Y. Hu, F. Lin, X. Zhang, *Water* **2024**, *16*, 553.
[30] M. E. Solmaz, A. Y. Mutlu, G. Alankus, V. Kilic, A. Bayram, N. Horzum, *Sens. Actuators, B* **2018**, *255*, 1967.
[31] M. Sugden, M. Holness, *Clin. Lipidol. Metab. Disord.* **2011**, *6*, 4.
[32] E. F. Carrizales-Sepúlveda, R. Vera-Pineda, R. A. Jiménez-Castillo, J. R. Violante-Cumpa, R. Flores-Ramrez, A. Ordaz-Faras, *Am. J. Med. Sci.* **2021**, *361*, 690.
[33] I. Kaiserman, N. Kaiserman, S. Nakar, S. Vinker, *Am. J. Ophthalmol.* **2005**, *139*, 498.
[34] S. Park, D. Y. Nam, H.-J. Jeon, J. H. Han, D. Jang, J. Hwang, Y.-S. Park, Y.-G. Han, Y. B. Choy, D. Y. Lee, *Biomater. Res.* **2023**, *27*, 135.
[35] J.-J. Luo, S.-W. Pan, J.-H. Yang, T.-L. Chang, P.-Y. Lin, C.-L. Wu, W.-F. Liu, X.-R. Huang, I. O. Koshevoy, P.-T. Chou, M.-L. Ho, *Polymers* **2018**, *10*, 1001.
[36] A. Poddar, N. Rangwani, S. Palekar, J. Kalambe, *Mater. Today: Proc.* **2023**, *73*, 100.
[37] S. Sajed, M. Kolahdouz, M. A. Sadeghi, *ChemistrySelect* **2022**, *7*, e202201376.
[38] R. Moreddu, J. S. Wolffsohn, D. Vigolo, A. K. Yetisen, *Sens. Actuators, B* **2020**, *317*, 128183.
[39] Z. Wang, Y. Dong, X. Sui, X. Shao, K. Li, H. Zhang, Z. Xu, D. Zhang, *npj Flexible Electron.* **2024**, *8*, 35.
[40] H. Zhang, E. Smith, W. Zhang, A. Zhou, *Biomed. Microdevices* **2019**, *21*, 48.
[41] F. Li, X. Wang, J. Liu, Y. Hu, J. He, *Sens. Actuators, B* **2019**, *288*, 266.
[42] D. Sen, G. Sarin, *Br. J. Ophthalmol.* **1980**, *64*, 693.
[43] M. B. Abelson, I. J. Udell, J. H. Weston, *Arch. Ophthalmol.* **1981**, *99*, 301.
[44] H. Song, H. Shin, H. Seo, W. Park, B. J. Joo, J. Kim, J. Kim, H. K. Kim, J. Kim, J.-U. Park, *Adv. Sci.* **2022**, *9*, 2203597.
[45] S. K. Srivastava, M. Bhaiyya, S. Dudala, C. Hota, S. Goel, *Sens. Actuators, A* **2023**, *350*, 114135.
[46] L. Silveira, R. D. C. F. Borges, R. S. Navarro, H. E. Giana, R. A. Zângaro, M. T. T. Pacheco, A. B. Fernandes, *Lasers Med. Sci.* **2017**, *32*, 787.
[47] M. Bhaiyya, S. K. Srivastava, P. K. Pattnaik, S. Goel, *IEEE Trans. Instrum. Meas.* **2023**, *72*, 9510308.
[48] C. L. Morais, K. M. Lima, F. L. Martin, *Anal. Lett.* **2018**, *51*, 2860.
[49] Q. Wang, G. Wu, F. Pian, P. Shan, Z. Li, Z. Ma, *Spectrochim. Acta, Part A* **2021**, *260*, 119906.
[50] A. Sharma, D. C. Weindorf, T. Man, A. A. A. Aldabaa, S. Chakraborty, *Geoderma* **2014**, *232*, 141.
[51] M. M. Elsenety, M. B. I. Mohamed, M. E. Sultan, B. A. Elsayed, *Sci. Rep.* **2022**, *12*, 22584.
[52] Y. Wang, Y. Liu, W. Liu, W. Tang, L. Shen, Z. Li, M. Fan, *Anal. Methods* **2018**, *10*, 3059.
[53] D. W. Hastuti, M. Harahap, F. A. Ferdiansyah, A. H. Saputro, C. Imawan, *J. Phys.: Conf. Ser.* **2020**, *1528*, 012050.